Remodeling of actin filaments by ADF/cofilin proteins

Vitold E. Galkin[a,1], Albina Orlova[a], Dmitri S. Kudryashov[b,2], Alexander Solodukhin[a], Emil Reisler[b], Gunnar F. Schröder[c], and Edward H. Egelman[a,1]

[a]Department of Biochemistry and Molecular Genetics, University of Virginia, Box 800733, Charlottesville, VA 22908-0733; [b]Department of Chemistry and Biochemistry and Molecular Biology Institute, University of California, 405 Hilgard Avenue, Los Angeles, CA 90095; and [c]Institute of Complex Systems (ICS-6), Forschungszentrum Jülich, 52425 Jülich, Germany

Edited by* David DeRosier, Brandeis University, Waltham, MA, and approved October 13, 2011 (received for review June 22, 2011)

Cofilin/ADF proteins play key roles in the dynamics of actin, one of the most abundant and highly conserved eukaryotic proteins. We used cryoelectron microscopy to generate a 9-Å resolution three-dimensional reconstruction of cofilin-decorated actin filaments, the highest resolution achieved for a complex of F-actin with an actin-binding protein. We show that the cofilin-induced change in the filament twist is due to a unique conformation of the actin molecule unrelated to any previously observed state. The changes between the actin protomer in naked F-actin and in the actin-cofilin filament are greater than the conformational changes between G- and F-actin. Our results show the structural plasticity of actin, suggest that other actin-binding proteins may also induce large but different conformational changes, and show that F-actin cannot be described by a single molecular model.

cytoskeleton | electron microscopy | helical polymers

Actin is essential for the survival of most cells because of its crucial role in cell division, locomotion, and mechanical support (1). Recent advances in X-ray fiber diffraction and electron cryomicroscopy (cryo-EM) revealed a "flattening" of the globular monomeric actin (G-actin) upon polymerization into filaments (F-actin) (2, 3) as well as showing a multiplicity of different structural states in F-actin (4). In the cell, actin interacts with more than 100 actin-binding proteins (ABPs) (1) that regulate the assembly and disassembly of different types of actin cytoskeletal networks. Despite the importance of these cellular interactions, our understanding of the alterations in F-actin structure upon interaction with ABPs is limited. A 9.5-Å resolution cryo-EM reconstruction of an actin–scruin bundle from *Limulus* sperm revealed very large deviations in the twist and tilt of the actin subunits from their ideal positions in F-actin (5). A three-dimensional (3D) reconstruction (at approximately 12 Å) of F-actin decorated with actin-binding domain 2 (ABD2) of fimbrin showed that the ATP-binding cleft of actin in the complex was more closed than that in the control undecorated actin filaments (6). In contrast, a 14 Å cryo-EM reconstruction of F-actin decorated with myosin Subfragment 1 did not reveal significant deviations in its structure from undecorated F-actin (7).

Cofilin/ADF proteins are essential and conserved modulators of actin dynamics in eukaryotic cells. While cofilin was originally viewed as a protein that severed and depolymerized actin filaments, it is now understood to play more diverse roles in regulating the assembly of cellular actin pools, including the formation of stable actin-cofilin rods that are associated with neurodegeneration (8). Recent findings demonstrate that the activity of cofilin is modulated by almost any perturbation of normal cell physiology (9) and identify this protein as a "functional node in cell biology" (9). However, our understanding of the cofilin-F-actin interaction is hampered by the absence of a high resolution structure of this complex.

Results

We used images (Fig. 1) of frozen-hydrated actin filaments extensively decorated with human cofilin-2 under conditions where there is limited depolymerization (pH 6.5) to extract 28,560 short segments (each containing 18 actin molecules). The single particle approach to helical reconstruction (10) allowed us to select 13,716 uniformly decorated segments (Fig. S1*A*) and these were used to generate a 3D reconstruction of cofilin-decorated F-actin (Fig. 1*C*, transparent surface). The Fourier shell correlation (FSC) approach to resolution determination yielded a resolution of 10.2 Å using the FSC = 0.5 criterion and 8.5 Å using the Henderson (11) criterion (FSC = 0.143) (Fig. S1*C*). Comparisons of the actual reconstruction with the electron density map of the atomic model filtered to different resolutions showed a best match at 9-Å resolution (Fig. S1*D*).

A flexible fitting procedure (12) was used to generate a pseudoatomic model (see *Materials and Methods*) of the cofilin-actin filament (Fig. 1*C*, ribbons) starting from a solution structure of human cofilin (13) and a crystal structure of actin (14). Cofilin interactions with the actin filament can be divided into two regions (15)—the upper site previously described as the G-actin-binding site and the lower site known as the F-actin-binding site (Fig. 2). The G-actin-binding site is composed of two major contacts, and the interface that we see is very similar to that described for a complex of twinfilin, a cofilin homolog, and G-actin (16). Actin residues 143–147 and 343–346 interact with cofilin residues 112–119 located on the top of the α4-helix (Fig. 2*A*). Yeast mutagenesis experiments revealed that the R96A and K98A substitutions in yeast cofilin (corresponding to K112 and K114 in human cofilin) are lethal (15), while peptide binding experiments mapped the G-actin-binding site of human cofilin to residues 136–143 and 346–353 of actin (17). The C-terminal residues of actin (349–354) form an extensive contact with the loop 41–46 and the N terminus of cofilin (Fig. 2*B*). Alanine substitutions in residues D34, K36 and E38 (residues E42, K44, and N46 in human cofilin) yield a mutant that is lethal for yeast, despite only small defects in F-actin depolymerization activity in vitro (15). Deletion of five N-terminal cofilin residues is also lethal in yeast, while deletion of these residues in porcine cofilin enables it to interact with phalloidin stabilized F-actin (in contrast to WT cofilin, which does not bind to phalloidin-actin) (18). Thus, the actin-binding region formed by cofilin residues 1–5 and 41–46 may not be required for cofilin attachment to the actin filament per se but rather may induce structural perturbations in F-actin that are crucial in the cell. This is consistent with the fact that the cofilin N terminus contains a critical phosphorylation site at Ser4 that regulates the activity of cofilin (19).

Author contributions: V.E.G., A.O., E.R., and E.H.E. designed research; V.E.G., A.O., A.S., and G.F.S. performed research; D.S.K., E.R., and G.F.S. contributed new reagents/analytic tools; V.E.G., G.F.S., and E.H.E. analyzed data; and V.E.G., A.O., E.R., and E.H.E. wrote the paper.

The authors declare no conflict of interest.

*This Direct Submission article had a prearranged editor.

Data deposition: The three-dimensional reconstruction has been deposited in the EM Data Bank (EMD-5354), and the atomic model has been deposited in the Protein Data Bank, www.pdb.org (PDB ID code 3J0S).

[1]To whom correspondence may be addressed. E-mail: galkin@virginia.edu or egelman@virginia.edu.

[2]Present address: Department of Biochemistry, Ohio State University, 484 West 12th Avenue, 728 Bioscience Building, Columbus, OH 43210.

This article contains supporting information online at www.pnas.org/lookup/suppl/doi:10.1073/pnas.1110109108/-/DCSupplemental.

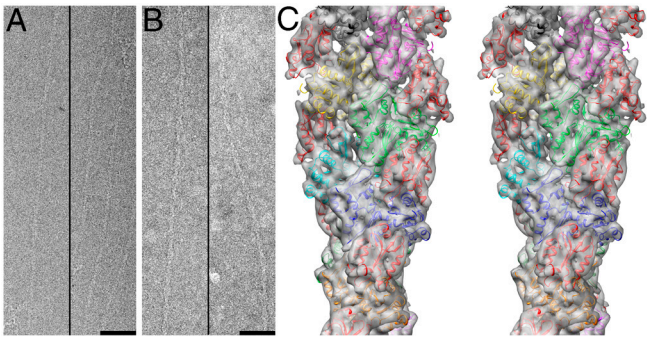

Fig. 1. (*A*) Pure actin filaments, imaged by cryo-EM, are thinner than (*B*) filaments decorated with cofilin-2. Scale bar, 500 Å. (*C*) Stereo view of the 3D reconstruction of F-actin decorated with cofilin-2 (transparent surface) is shown with the corresponding pseudoatomic model of the complex (ribbons). Cofilin molecules are in red.

The F-actin-binding site of cofilin also has two separate contacts. The first contact between the small loop of cofilin (residues 154–158) is formed with actin residues 242–243 located at the top of Subdomain 4 (SD4) (Fig. 2*C*). Interaction of cofilin with the 241–245 loop of actin, a loop that is crucial to maintaining the integrity of the filament (3, 4, 20), has never been reported. Mutations in residues E134, R135, and R138 of yeast cofilin (A150, E151, and G154 in human cofilin) yield a protein that readily binds to G-actin but has reduced affinity for F-actin (15). The second site involves cofilin residues 94–98 forming an extensive contact with residues 21–28 and 90–96 within SD1 of actin (Fig. 2*D*). The R80A and K82A mutants in yeast cofilin (K96 and D98 in human cofilin) possess weak F-actin-binding, impaired depolymerization activity and are lethal in yeast (15). Residues 19–21 of cofilin located in the α1-helix interact with residues 90–96 of actin (Fig. 2*D*). At the current resolution there is a unique orientation of cofilin on actin. In contrast, with a substantially lower resolution reconstruction of cofilin-decorated actin we stated that a unique model was not possible (21).

Cofilin has been shown (22) to change the helical twist of F-actin by 5° between protomer n and $n+1$. Thus, when cofilin is bound the rotation between protomer n and $n+2$ along the

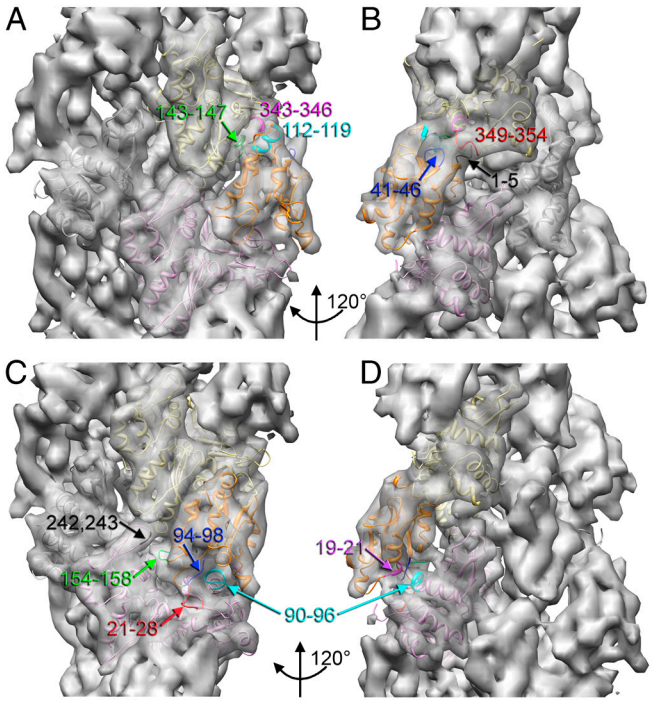

Fig. 2. Cofilin forms four contacts with two adjacent actin protomers. (*A*) Actin residues 143–147 (green) and 343–346 (magenta) interact with cofilin residues 112–119 (cyan). (*B*) The C-terminal residues 349–354 (red) form a bridge of density with a loop 41–46 (blue) and the N terminus (residues 1–5 in black) of cofilin. (*C*) A small loop 154–158 (green) in cofilin contacts residues 242 and 243 (black) of actin, while cofilin residues 94–98 (blue) interact with residues 21–28 (red) and 90–96 (cyan) within SD1 of actin. (*D*) Residues 19–21 (magenta) of cofilin also make a contact with residues 90–96 (cyan) of actin.

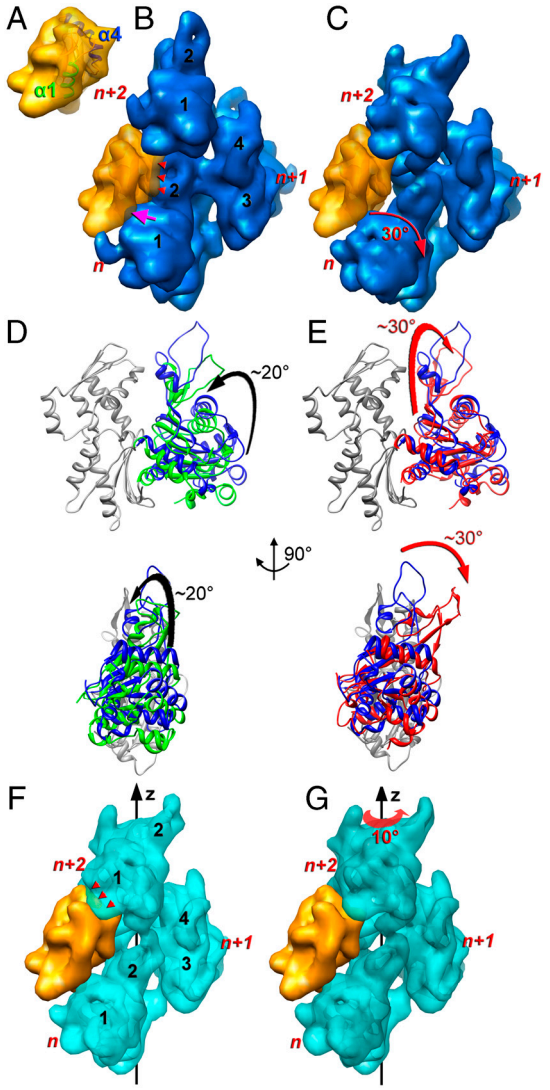

Fig. 3. Cofilin alters the conformation of actin protomers and the helical twist of the actin filament. When a cofilin molecule (*A*) is placed on the surface of the unperturbed actin filament (*B*) the α1-helix (green) of cofilin clashes with the SD1 of actin (magenta arrow), while the α4-helix (blue) has a steric clash with SD2 of actin (red arrowheads). (*C*) Rotation of the outer domain of actin by approximately 30° (red arrow) resolves these clashes. (*D*) The inner domain of actin (SD3 and SD4) is shown in gray, while the outer domain is colored. Rotation of the outer domain from G-actin conformation (green ribbons) to F-actin conformation (blue ribbons) by approximately 20° (black arrow) flattens the actin molecule. (*E*) Upon cofilin binding, the outer domain of actin rotates from the F-actin conformation (blue ribbons) by approximately 30° (red arrow) toward the opposite helical strand (red ribbons). (*F*) When cofilin-deformed actin protomers (*E*) are arranged into a helical filament having the normal symmetry (*F*), the α4-helix of cofilin clashes with the lower portion of SD1 of actin (red arrowheads). (*G*) The clash shown in *F* can be resolved by rotation of protomer $n+2$ by 10° around the helical axis (red arrow).

same strand is changed by 10°. When such a twist change is imposed upon the original structural state of F-actin (3) (Fig. 3*B*) cofilin cannot preserve its contacts with two actin protomers because of two steric clashes—one between the α1-helix of cofilin with the SD1 of actin (Fig. 3*B*, magenta arrow), and the other between the α4-helix of cofilin and SD2 of actin (Fig. 3*B*, red arrowheads). To overcome these clashes all actin protomers in the cofilactin filament are found in a new structural state in which the outer domain of each subunit (SD1 and SD2) rotates toward the opposite helical strand (Fig. 3*C*). Such a structural state of actin has never been observed in either G-actin or actin filaments, either naked or decorated with ABPs. Upon polymerization of G-actin into F-actin the outer domain of actin rotates by approximately 20°, which flattens the actin molecule (3) (Fig. 3*D*); the attachment of cofilin to the actin filament rotates the outer domain of the actin molecule from its flattened position toward the opposite helical strand by approximately 30° (Movie S1).

The sorting procedure that classified segments used for the reconstruction discussed thus far (see *Materials and Methods*) also showed the existence of other classes of structures. We characterized approximately 17% of segments of cofilactin filaments as having SD2 of actin completely disordered and thus not visible in a 3D reconstruction (Fig. S1*A*). The orientation of SD1 of actin in the reconstruction of this class (Fig. S2) is the same as in the uniformly occupied set (Fig. 1*C*). This suggests that the specific interaction between cofilin and SD1 of actin (Fig. 2) twists SD1 toward the opposite helical strand, while SD2 follows suit due to mechanical association with SD1.

We also examined whether cofilin can bind to an actin filament model composed of "morphed" actin protomers arranged into a filament with a normal twist of 26° between the n and $n+2$ protomers (−167° between the n and $n+1$ subunits), as opposed to the actual cofilactin filaments, which have a twist of 36° between protomers n and $n+2$ (and a twist of −162° between protomers n and $n+1$). Our modeling shows that in this case the α4-helix of cofilin clashes with the lower portion of SD1 (Fig. 3*F*, red arrowheads). To avoid these steric clashes between actin and cofilin, actin protomer $n+2$ needs to be twisted by approximately 10° with respect to subunit n (Fig. 3*G*). This is possible due to the extensively described variability in twist within F-actin (23, 24).

The rotation of the outer domain of actin upon cofilin binding alters the longitudinal contacts between actin protomers (Fig. 4). At 9-Å resolution our modeling suggests that the interface between the SD3 and SD4 remains similar to that in the regular state of F-actin (3) (Fig. 4, green and yellow spheres). In contrast, the interface between SD1 and SD2 of two adjacent protomers is altered in the cofilactin filament due to the approximately 30° rotation of the outer domain of actin (Fig. 4, red and blue spheres). A previously proposed model for the cofilin-actin filament rotated the entire actin subunit to avoid the steric clash between cofilin and actin's subdomain 2 (16). The interaction between residues 40, 45, 61, 62, and 64 of the lower actin protomer with their counterparts in SD1 (143, 166, 167, and 169) of the protomer above it is broken, while a novel contact between Val45 and the C terminus of the adjacent protomer (Fig. 4, cyan ribbons) is established. These results support our previous observation, made at much lower resolution, that cofilin weakens the longitudinal contact between SD1 and SD2 of adjacent actin subunits (21). The breakage of the interaction between Arg62 and Asp288 upon rotation of the outer domain of actin provides a simple explanation for the acceleration in the presence of cofilin of the cleavage of SD2 at Arg62 by trypsin (25). Displace-

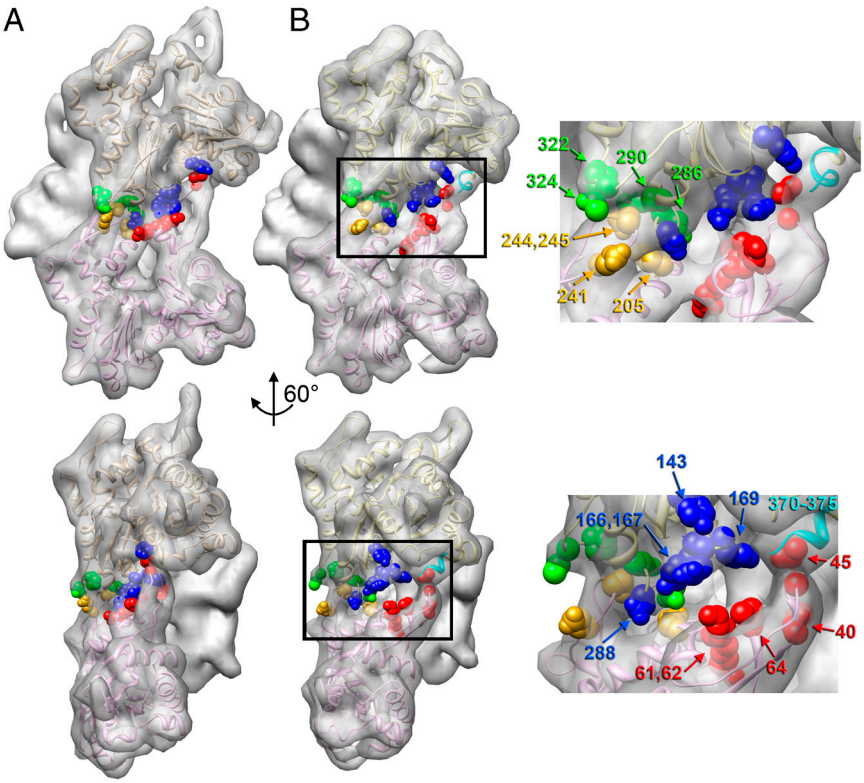

Fig. 4. Cofilin alters F-actin longitudinal contacts. The residues involved in contacts between the two adjacent actin protomers (plum and tan ribbons) in regular actin (*A*) and cofilactin filaments (*B*) are shown as colored spheres. The interface between SD3 and SD4 (yellow and green spheres) is not altered by cofilin and includes interactions between Glu205, Asp241, Asp244, and Glu245 (yellow) with Asp286, Thr324, Arg290, and Pro322 (green), respectively. In regular actin (*A*) residues His40, Val45, Lys61, Arg62, and Ile64 (red) form bonds with Tyr169, Tyr143, Glu167, Asp288, and Tyr166 (blue), respectively. Rotation of the outer domain of actin upon cofilin binding (*B*) disrupts all of the above bonds and introduces a bridge of density between Val45 and the C terminus of actin (residues 370–375 in cyan).

ment of SD2 of actin upon cofilin binding increases the distance between residues 41 and 374 of two adjacent actin protomers by 3 Å, consistent with reduction in the formation of a disulfide bond between these residues in the presence of cofilin (26).

Discussion

In a recent paper (4) we showed that F-actin is intrinsically polymorphic, and suggested that the couplings in structural changes are part of an extensive allosteric network within actin. Such allosteric couplings must place constraints on the buried actin residues (27), helping to explain the anomalous sequence conservation in actin. The unique alterations in actin structure observed in the presence of cofilin extend our knowledge about the plasticity of the actin molecule and suggest that other ABPs may induce large but different conformational changes in F-actin. A multiplicity of actin conformational states induced by different actin-nucleating proteins (28–31) and ABPs may allow cells to distinguish between different actin filaments. For example, if the same conformational changes are present in actin in the stable actin-cofilin rods observed in neurodegenerative diseases (8), many actin-binding proteins might not be able to interact with such actin filaments.

As we have shown here, cofilin can both substantially displace subdomain 2 of actin as well as cause it to be disordered. We have previously shown that a disordering of subdomain 2 leads to a fourfold increase in the flexibility of the actin filament (32), and the cofilin-induced increase in F-actin flexibility by a similar amount has already been reported (33). This change in F-actin flexibility makes simple physical sense because the resistance to bending will scale as the fourth power of the radial mass distribution, and subdomain 2 forms the highest radius contact in the filament. One can reasonably imagine that the measured (34–37) persistence length of actin filaments (a quantification of the flexural rigidity) arises from a mixture of the many states observed in Galkin et al. (4). Under conditions where subdomain 2 is more disordered, the filaments become much more flexible, just as one would expect that under conditions where subdomain 2 becomes more ordered the filaments become more rigid (3).

What does the model of cofilin-induced structural changes in F-actin tell us about how cofilin severs actin filaments? A recent paper has shown that cofilin severs F-actin at the junction between bare and decorated regions (38). In the decorated regions cofilin is disrupting the longitudinal interface in the filament but also forming a cross-link that maintains this bond. The cofilin-induced changes in subdomain 2 of F-actin cooperatively propagate into the undecorated regions, but the absence of cofilin in these regions means that the filament will not be stable. The cooperative propagation of conformational changes in F-actin has been extensively observed (28, 39–41).

Finally, we suggest that conformational changes within F-actin of a magnitude similar to what is observed with cofilin binding may be necessary to understand the actomyosin force-generation cycle because modifications of actin that do not affect myosin binding or actin's activation of the myosin ATPase have been shown to greatly reduce or eliminate force generation (42–44). It is interesting that some of these modifications place constraints on the dynamics of the SD2-SD1 interface in the actin filament, a region that we show here is quite labile.

Materials and Methods

Sample Preparation and Electron Microscopy. Skeletal muscle G-actin [10 μM] was polymerized in F buffer (20 mM Pipes-buffer, pH 6.5, 40 mM KCl, 1 mM $MgCl_2$, 4 mM DTT, and 0.5 mM ATP) overnight at 4 °C. F-actin was collected in a TLX-Beckman centrifuge (50,000 rpm for 45 min) and homogenized in the F buffer without ATP.

The DNA sequence of human cofilin-2 was amplified from a human cDNA library (Invitrogen) using the following set of primers: forward [5′-attacatggcttctggagttacagtg-3′] and reverse [5′-taggatccttataatggttttccttcaagtg-3′], containing *NcoI* and *BamHI* restriction sites, respectively. The PCR product was cloned into pET15b vector (Novagen) and expressed in BL21 (DE3) strain of *E.coli*. Cells were grown at 37 °C to a density of 0.8 absorbance units and then cooled to 25 °C. Protein expression was induced with 1 mM IPTG overnight. Cells were harvested by centrifugation and resuspended in 20 mM TRIS-HCl (pH 7.5), 1 mM DTT, 0.2 mM PMSF buffer (extraction buffer) supplemented with a cocktail of protease inhibitors (Roche). Cells were lysed by sonication and clarified by centrifugation. The clarified supernatant was applied to a QAE-52 column (16 × 250 mm; GE Healthcare) equilibrated with an extraction buffer. Cofilin-2 was collected in a flow-through fraction of the QAE-52 column. The flow-through fraction was collected, supplemented with 200 mM NaCl and concentrated to 2 mls (using centrifugal concentrators, Amicon). It was applied then to a Superdex-75 16/60 column (GE Healthcare) equilibrated with the extraction buffer supplemented with 200 mM NaCl. Peak fractions containing cofilin-2 were pooled, concentrated and dialyzed against the extraction buffer. The concentration of cofilin-2 was determined spectrophotometrically using A(0.1%) at 280 nm of 0.985 cm^{-1}.

F-actin [4–5 μM] in F buffer was incubated with human cofilin-2 [15–20 μM] for 20–40 min. Cryosamples were prepared using a Vitrobot Mark IV (Gatan) plunge freezer. Droplets (2–2.5 μL) were applied to glow-discharged C-Flat grids with 100% humidity at 10 °C. All cryo-EM was done on a Tecnai F20 microscope operated at 200 keV at a magnification of 50,000×. Images were recorded on film with defocus values from 1.1–5.3 μ.

Image Processing. The SPIDER software package (45) was used for most image processing, but the EMAN package (46) was used to extract filament images from micrographs and the BSOFT package (47) was used to determine defocus values.

A Nikon COOLPIX 8000 scanner was used to digitize 125 cryo-EMs at a raster of 1.25 Å per pixel. Initial correction for the contrast transfer function (CTF) was made by multiplying each image by its theoretical CTF. From these CTF-corrected images, 28,560 short (400 pixel long) overlapping segments were extracted. The segments were down-sampled to 2.5 Å per pixel and reconstructed using the IHRSR method (10). The volume was corrected for the CTF by using a Wiener filter assuming that the signal-to-noise ratio in the volume was very large, and a negative B-factor of 1,150 was used to amplify high frequencies in the reconstruction. The volume was initially filtered to 10-Å resolution. The UCSF Chimera software (48) was used to fit the solution structure of human cofilin (13) along with the structure of the actin protomer from the model of the actin filament in the "regular" state (3) into the experimental map. The resultant atomic model was then perturbed in various ways and used for cross-correlation sorting of the images.

Five models were created. The first model had actin protomers in the "regular" state but twisted to −162°; the next two models had the cofilin molecule tilted away from its position in the uniformly decorated filament model by 15° with the upper or lower contacts with the actin filament disrupted; the fourth was the unperturbed model of the uniformly decorated filament; a fifth model was the same as the fourth but with a missing subdomain 2 (SD2). These volumes were scaled to 5.0 Å per pixel and projected onto 100 × 100 px images with azimuthal rotational increments of 4°, generating 450 reference projections (5 × 90). The 28,560 cofilactin segments were down-sampled to 5.0 Å per pixel and cross-correlated with the 450 reference projections. A set of 13,716 segments (48%) was selected as similar to the uniformly decorated state, while 4,072 segments were assigned to the SD2-disordered class (14%) (Fig. S1*A*). Both sets (sampled at 2.5 Å per pixel) were reconstructed with the IHRSR method. After approximately 30 iterations both sets converged to the same solution of −162.1°/27.6 Å. These two volumes were corrected for the CTF as described previously. The uniformly decorated volume was filtered to 9.0-Å resolution (Fig. 1*C*), while the one with SD2 disordered was filtered to 10.0 Å (Fig. S2).

To test for the possibility of model bias, a sixth "bogus" model was created that was missing subdomain 1. When the sorting was redone using these six models, only approximately 2% of the segments were selected as most similar to the bogus model. In contrast, the smallest cofilin-bound subset (with SD2 disordered) had 14% of the images. When this small set was used in IHRSR with a solid cylinder as a starting reference, it went to a strange symmetry of −161.1° with a 30.3 Å axial rise per subunit (in contrast to the symmetry of the bogus model, −162.1° and 27.6 Å). A comparison between the model and the resulting reconstruction showed no significant similarity.

Model Creation and Structure Refinement. For both density maps the same starting model was used for the refinement. The actin monomer structure was taken from PDB ID code 2BTF and the cofilin monomer was taken from PDB ID code 1Q8G. Atomic coordinates from these high-resolution structures were converted to density maps, filtered to the resolution of the experimental map, and docked into the maps using the UCSF Chimera software. The

experimentally determined helical symmetry of −162.1°/27.6 Å was applied to yield a system of nine actin and 10 cofilin protomers with 39,213 atoms in total as a starting point for the flexible refinement. The program CNS (50) was then used to correct the broken linkages between the fragments and remove atom clashes by energy minimization of the whole structure. During this minimization the fragments were strongly restrained, which moved them almost as rigid bodies. The starting models obtained by this procedure were then subjected to real-space refinement against the density map using the program DireX (12). An elastic network potential was used during the refinement, where in total 78,426 (two times the number of atoms) harmonic restraints where randomly chosen from the list of atom pairs that are initially within a distance of 3 to 15 Å and are separated along the main chain by not more than 30 residues. There were no restraints between the different monomers. It should be noted that the elastic network was in this case chosen not to be deformable (i.e., the gamma value was set to zero). Elastic restraints within secondary structure elements were weighted twice as strong as in loop regions. The secondary structure assignment was computed using DSSP (49).

The DireX refinement was performed in two steps, first 200 steps of positional refinement with a large stepsize to quickly move the model into the density, followed by 2,000 steps of small step-size refinement together with occupancy refinement. The occupancy is a value between 0 and 1 and scales the weight of each atom in the computation of the model density map to account for missing or reduced density due to flexible parts of the molecule. The refined structure was then further optimized using CNS software (50) with 1,000 steps of Cartesian dynamics at a temperature of 30 K followed by 300 steps minimization. For both dynamics and minimization all hydrogen atoms were added to the model and electrostatic interaction was used between backbone atoms only to improve the hydrogen bonding network. In addition, statistical Ramachandran restraints were used to improve the backbone dihedral angles.

ACKNOWLEDGMENTS. This work was supported by National Institutes of Health Grants GM081303 (E.H.E.) and GM077190 (E.R.).

1. Pollard TD, Cooper JA (2009) Actin, a central player in cell shape and movement. *Science* 326:1208–1212.
2. Oda T, Iwasa M, Aihara T, Maeda Y, Narita A (2009) The nature of the globular- to fibrous-actin transition. *Nature* 457:441–445.
3. Fujii T, Iwane AH, Yanagida T, Namba K (2010) Direct visualization of secondary structures of F-actin by electron cryomicroscopy. *Nature* 467:724–728.
4. Galkin VE, Orlova A, Schroder GF, Egelman EH (2010) Structural polymorphism in F-actin. *Nat Struct Mol Biol* 17:1318–1323.
5. Schmid MF, Sherman MB, Matsudaira P, Chiu W (2004) Structure of the acrosomal bundle. *Nature* 431:104–107.
6. Galkin VE, Orlova A, Cherepanova O, Lebart MC, Egelman EH (2008) High-resolution cryo-EM structure of the F-actin-fimbrin/plastin ABD2 complex. *Proc Natl Acad Sci USA* 105:1494–1498.
7. Holmes KC, Angert I, Kull FJ, Jahn W, Schroder RR (2003) Electron cryo-microscopy shows how strong binding of myosin to actin releases nucleotide. *Nature* 425:423–427.
8. Bamburg JR, et al. (2010) ADF/Cofilin-actin rods in neurodegenerative diseases. *Curr Alzheimer Res* 7:241–250.
9. Bernstein BW, Bamburg JR (2010) ADF/cofilin: A functional node in cell biology. *Trends Cell Biol* 20:187–195.
10. Egelman EH (2000) A robust algorithm for the reconstruction of helical filaments using single-particle methods. *Ultramicroscopy* 85:225–234.
11. Rosenthal PB, Henderson R (2003) Optimal determination of particle orientation, absolute hand, and contrast loss in single-particle electron cryomicroscopy. *J Mol Biol* 333:721–745.
12. Schroder GF, Brunger AT, Levitt M (2007) Combining efficient conformational sampling with a deformable elastic network model facilitates structure refinement at low resolution. *Structure* 15:1630–1641.
13. Pope BJ, Zierler-Gould KM, Kuhne R, Weeds AG, Ball LJ (2004) Solution structure of human cofilin: Actin binding, pH sensitivity, and relationship to actin-depolymerizing factor. *J Biol Chem* 279:4840–4848.
14. Schutt CE, Myslik JC, Rozycki MD, Goonesekere NCW, Lindberg U (1993) The structure of crystalline profilin:β-actin. *Nature* 365:810–816.
15. Lappalainen P, Fedorov EV, Fedorov AA, Almo SC, Drubin DG (1997) Essential functions and actin-binding surfaces of yeast cofilin revealed by systematic mutagenesis. *EMBO J* 16:5520–5530.
16. Paavilainen VO, Oksanen E, Goldman A, Lappalainen P (2008) Structure of the actin-depolymerizing factor homology domain in complex with actin. *J Cell Biol* 182:51–59.
17. Mannherz HG, et al. (2007) Mapping the ADF/cofilin binding site on monomeric actin by competitive cross-linking and peptide array: Evidence for a second binding site on monomeric actin. *J Mol Biol* 366:745–755.
18. Moriyama K, Yahara I (2002) The actin-severing activity of cofilin is exerted by the interplay of three distinct sites on cofilin and essential for cell viability. *Biochem J* 365:147–155.
19. Morgan TE, Lockerbie RO, Minamide LS, Browning MD, Bamburg JR (1993) Isolation and characterization of a regulated form of actin depolymerizing factor. *J Cell Biol* 122:623–633.
20. Rould MA, Wan Q, Joel PB, Lowey S, Trybus KM (2006) Crystal structures of expressed non-polymerizable monomeric actin in the ADP and ATP states. *J Biol Chem* 281:31909–31919.
21. Galkin VE, et al. (2003) ADF/cofilin use an intrinsic mode of F-actin instability to disrupt actin filaments. *J Cell Biol* 163:1057–1066.
22. McGough A, Pope B, Chiu W, Weeds A (1997) Cofilin changes the twist of F-actin: Implications for actin filament dynamics and cellular function. *J Cell Biol* 138:771–781.
23. Egelman EH, Francis N, DeRosier DJ (1982) F-actin is a helix with a random variable twist. *Nature* 298:131–135.
24. Schmid MF, Sherman MB, Matsudaira P, Chiu W (2004) Structure of the acrosomal bundle. *Nature* 431:104–107.
25. Muhlrad A, et al. (2004) Cofilin induced conformational changes in F-actin expose subdomain 2 to proteolysis. *J Mol Biol* 342:1559–1567.
26. Bobkov AA, et al. (2002) Structural effects of cofilin on longitudinal contacts in F-actin. *J Mol Biol* 323:739–750.
27. Suel GM, Lockless SW, Wall MA, Ranganathan R (2003) Evolutionarily conserved networks of residues mediate allosteric communication in proteins. *Nat Struct Biol* 10:59–69.
28. Orlova A, Prochniewicz E, Egelman EH (1995) Structural dynamics of F-actin. II. Cooperativity in structural transitions. *J Mol Biol* 245:598–607.
29. Prochniewicz E, Zhang Q, Janmey PA, Thomas DD (1996) Cooperativity in F-actin: Binding of gelsolin at the barbed end affects structure and dynamics of the whole filament. *J Mol Biol* 260:756–766.
30. Khaitlina S, Hinssen H (1997) Conformational changes in actin induced by its interaction with gelsolin. *Biophys J* 73:929–937.
31. Bugyi B, et al. (2006) Formins regulate actin filament flexibility through long range allosteric interactions. *J Biol Chem* 281:10727–10736.
32. Orlova A, Egelman EH (1993) A conformational change in the actin subunit can change the flexibility of the actin filament. *J Mol Biol* 232:334–341.
33. McCullough BR, Blanchoin L, Martiel JL, De La Cruz EM (2008) Cofilin increases the bending flexibility of actin filaments: Implications for severing and cell mechanics. *J Mol Biol* 381:550–558.
34. Dupuis DE, Guilford WH, Wu J, Warshaw DM (1997) Actin filament mechanics in the laser trap. *J Muscle Res Cell Motil* 18:17–30.
35. Gittes F, Mickey B, Nettleton J, Howard J (1993) Flexural rigidity of microtubules and actin filaments measured from thermal fluctuations in shape. *J Cell Biol* 120:923–934.
36. van MJ, Vermeulen KC, Gittes F, Schmidt CF (2009) Leveraging single protein polymers to measure flexural rigidity. *J Phys Chem B* 113:3837–3844.
37. Isambert H, et al. (1995) Flexibility of actin filaments derived from thermal fluctuations. Effect of bound nucleotide, phalloidin, and muscle regulatory proteins. *J Biol Chem* 270:11437–11444.
38. Suarez C, et al. (2011) Cofilin tunes the nucleotide state of actin filaments and severs at bare and decorated segment boundaries. *Curr Biol* 21:862–868.
39. Drewes G, Faulstich H (1993) Cooperative effects on filament stability in actin modified at the C-terminus by substitution or truncation. *Eur J Biochem* 212:247–253.
40. Prochniewicz E, Katayama E, Yanagida T, Thomas DD (1993) Cooperativity in F-actin: Chemical modifications of actin monomers affect the functional interactions of myosin with unmodified monomers in the same actin filament. *Biophys J* 65:113–123.
41. Bobkov AA, et al. (2006) Cooperative effects of cofilin (ADF) on actin structure suggest allosteric mechanism of cofilin function. *J Mol Biol* 356:325–334.
42. Kim E, Bobkova E, Hegyi G, Muhlrad A, Reisler E (2002) Actin cross-linking and inhibition of the actomyosin motor. *Biochemistry* 41:86–93.
43. Schwyter DH, Kron SJ, Toyoshima YY, Spudich JA, Reisler E (1990) Subtilisin cleavage of actin inhibits in vitro siding movement of actin filaments over myosin. *J Cell Biol* 111:465–470.
44. Prochniewicz E, Yanagida T (1990) Inhibition of sliding movement of F-actin by cross-linking emphasizes the role of actin structure in the mechanism of motility. *J Mol Biol* 216:761–772.
45. Frank J, et al. (1996) SPIDER and WEB: Processing and visualization of images in 3D electron microscopy and related fields. *J Struct Biol* 116:190–199.
46. Ludtke SJ, Baldwin PR, Chiu W (1999) EMAN: Semiautomated software for high-resolution single-particle reconstructions. *J Struct Biol* 128:82–97.
47. Heymann JB, Belnap DM (2007) Bsoft: Image processing and molecular modeling for electron microscopy. *J Struct Biol* 157:3–18.
48. Pettersen EF, et al. (2004) UCSF Chimera—a visualization system for exploratory research and analysis. *J Comput Chem* 25:1605–1612.
49. Kabsch W, Sander C (1983) Dictionary of protein secondary structure: Pattern recognition of hydrogen-bonded and geometrical features. *Biopolymers* 22:2577–2637.
50. Brunger AT, et al. (1998) Crystallography & NMR system: A new software suite for macromolecular structure determination. *Acta Crystallogr D Biol Crystallogr* 54:905–921.